View metadata, citation and similar papers at core.ac.uk

brought to you by CORE

provided by HZB Repository

Band offsets at κ-($[Al,In]_xGa_{1-x})_2O_3$/MgO interfaces

Thorsten Schultz[1,2*], Max Kneiß[3*], Philipp Storm[3], Daniel Splith[3], Holger von Wenckstern[3], Marius Grundmann[3], Norbert Koch[1,2]

[1]*Humboldt-Universität zu Berlin, Institut für Physik, 12489 Berlin, Germany*

[2]*Helmholtz-Zentrum für Energie und Materialien GmbH, 14109 Berlin, Germany*

[3]*Universität Leipzig, Felix-Bloch-Institut für Festkörperphysik, 04103 Leipzig, Germany*

[*]These authors contributed equally to this work.

E-mail corresponding author: tschultz@physik.hu-berlin.de

Abstract

Conduction and valence band offsets are amongst the most crucial material parameters for semiconductor heterostructure device design, such as for high-electron mobility transistors or quantum-well infrared photodetectors. Due to its expected high spontaneous electrical polarization and the possibility of polarization doping at heterointerfaces similar to the AlGaN/InGaN/GaN system, the metastable orthorhombic κ-phase of Ga_2O_3 and its indium and aluminum alloy systems are a promising alternative for such device applications. However, respective band offsets to any dielectric are unknown, as well as the evolution of the bands within the alloy systems. We report on valence and conduction band offsets of orthorhombic κ-$(Al_xGa_{1-x})_2O_3$ and κ-$(In_xGa_{1-x})_2O_3$ thin films to MgO as reference dielectric by X-ray photoelectron spectroscopy. The thin films with compositions $x_{In} \leq 0.27$ and $x_{Al} \leq 0.55$ were grown by pulsed laser deposition utilizing tin-doped and radially-segmented targets. The determined band alignments reveal the formation of a type I heterojunction to MgO for all compositions with conduction band offsets of at least 1.4 eV, providing excellent electron confinement. Only low valence band offsets with a maximum of ~300 meV were observed. Nevertheless, this renders MgO as promising gate dielectric for metal-oxide-semiconductor transistors in the orthorhombic modification. We further found that the conduction band offsets in the alloy systems are mainly determined by the evolution of the bandgaps, which can be tuned by the composition in a wide range between 4.1 and 6.2 eV, since the energy position of the valence band maximum stays almost constant over the complete composition range investigated. Therefore, tunable conduction band offsets of up to 1.1 eV within the alloy systems allow for subniveau transition energies in $(Al_xGa_{1-}x)_2O_3$/$(In_xGa_{1-x})_2O_3$/$(Al_xGa_{1-x})_2O_3$ quantum wells from the IR to the visible regime, which are promising for application in quantum-well infrared photodetectors.

Keywords: κ-Ga_2O_3, PLD, energy level alignment, band offsets, X-ray photoelectron spectroscopy

Introduction

The wide bandgap semiconductor Ga_2O_3 triggered enormous research efforts in recent years regarding potential device applications in power electronics and sensing. This is due to its large bandgap of 4.5-5.1 eV and consequently its large predicted electric breakdown field of about 8 MV/cm in the monoclinic modification, surpassing that of established materials such as SiC or GaN[1]. The availability of commercial 2", and recently also 4", single crystal β-Ga_2O_3 wafers grown from a melt stimulated these efforts additionally and several reviews dealt with the application of the thermodynamically stable monoclinic β-phase[1–4]. However, in the last years growing interest in the metastable phases of Ga_2O_3 emerged. Especially the frequency of reports on the orthorhombic κ-modification (sometimes also referred to as ε-Ga_2O_3) is rapidly increasing lately. Among the polymorphs of Ga_2O_3, this is the only crystalline phase expected to exhibit a spontaneous electrical polarization along its c-direction that is predicted to surpass even the one of GaN by one order of magnitude (23 μC/cm^2)[5–8]. The latter is the reason for the tremendously increasing interest in this phase. The GaN, AlGaN, and InGaN system is already established for applications such as high electron mobility transistors (HEMT)[9,10] or quantum-well infrared photodetectors (QWIP)[11] that utilize two dimensional electron gases (2DEGs) as active layer of the device. Such 2DEGs feature both high carrier densities as well as mobilities and can be realized in the GaN system solely by polarization doping, i.e. polarization differences at the interface of GaN/AlGaN or GaN/InGaN heterostructures cause polarization charges that result in band bending, localizing the 2DEG. The same then holds true for the orthorhombic modification of Ga_2O_3 only with even higher expected sheet charge carrier densities at the interfaces to κ-$(In_xGa_{1-x})_2O_3$ or κ-$(Al_xGa_{1-x})_2O_3$. HEMT structures and quantum wells containing 2DEGs are also possible in the monoclinic modification[12–17]. However, they always require a delta-doped layer containing e.g. Si that needs to be carefully designed in both concentration as well as distance to the heterointerface of the alloy system[12–14,16]. These complications would not be necessary in the orthorhombic modification.

The κ-phase of Ga_2O_3 has already been reported as thin film deposited by several different methods, including pulsed-laser deposition (PLD)[18–25], halide vapor phase epitaxy[26,27], metal-organic chemical vapor deposition[28–33], metal-organic vapor phase epitaxy[34–37], mist chemical vapor deposition (mist CVD)[38–42], molecular beam epitaxy (MBE)[43,44] and others. Recently, one report even achieved conductive doping of this phase by Si or Sn incorporation, which is necessary for a variety of device applications[36]. However, in PLD and MBE growth, tin is necessary as catalyst to stabilize the orthorhombic modification at all, but is not incorporated in the thin film layer as active donor element[18–20,23–25,44]. Further, several reports already deal with the alloying of this phase with indium[23,25,38] or aluminum[24,40] in a broad composition range, including bandgap engineering and the evolution of lattice constants. However, other crucial alloy properties for 2DEG device design are up to this day mostly unknown, the most critical ones are the evolution of the electrical polarization upon In- or Al-incorporation as well as band offsets for the design of both HEMT devices as well as quantum well heterostructures. To the best of the authors knowledge, only one report deals with band offsets in the κ-$(Al_xGa_{1-x})_2O_3$ system for mist CVD grown layers that were determined by X-ray photoelectron spectroscopy (XPS) measurements in a limited composition range[40].

This report seeks to fill this fundamental gap both in the In- as well as in the Al-alloy system of the orthorhombic modification, at least with respect to the band offsets. For this, phase pure thin films of κ-$(In_xGa_{1-x})_2O_3$ and κ-$(Al_xGa_{1-x})_2O_3$ in a broad composition range ($x_{In} \leq 0.27$ and $x_{Al} \leq 0.55$) were grown on κ-Ga_2O_3 buffer layers on c-sapphire substrates by vertical continuous composition spread PLD (VCCS PLD)[45]. As reference dielectric, MgO (111) layers with less than 10 nm thickness were deposited onto the alloy layers by PLD. The bandgaps of the alloy layers as well as valence and conduction band offsets to MgO were determined by XPS. MgO was found to provide excellent carrier confinement in the conduction band, forming heterostructures of type I in the complete composition range ($\Delta E_c > 1.4$ eV). However, only small valence band offsets can be realized. Heterostructures of the alloy systems are therefore expected to form type I interfaces as well, where the changing bandgap mainly causes a tunable shift in the conduction band offset with a flat evolution of the valence band edges. These results render the orthorhombic modification promising for heterostructure device applications.

Methods

Sample Preparation

The investigated κ-$(In_xGa_{1-x})_2O_3$ and κ-$(Al_xGa_{1-x})_2O_3$ layers, as well as the κ-Ga_2O_3 growth template and the MgO dielectric layer were grown by PLD. To vary the composition of the alloy layers, radially-segmented targets were employed and the respective layers were grown from these targets utilizing VCCS PLD. This technique, originally intended to realize composition gradients in growth direction of a thin film layer, is also able to produce laterally homogeneous alloy layers with any well-defined cation ratio to perform a discrete compositional screening. The variation and control of the alloy composition is accomplished by the respective fixed radial position *r* of the PLD laser spot on the employed elliptically-segmented target. A detailed description of this technique can be found in Reference[45]. The targets were either homogeneous Ga_2O_3 + 1 wt.% SnO_2 or MgO targets for the κ-Ga_2O_3 template layer or the MgO dielectric layer, respectively. The elliptically-segmented target for the κ-$(In_xGa_{1-x})_2O_3$ alloy layers was a $(In_{0.4}Ga_{0.6})_2O_3/Ga_2O_3$ target with additional 1.5 at.% SnO_2 in each segment and for the κ-$(Al_xGa_{1-x})_2O_3$ alloy layers a $(Al_{0.4}Ga_{0.6})_2O_3/Ga_2O_3$ or a $(Al_{0.2}Ga_{0.6})_2O_3/Ga_2O_3$ target with additional 2 at.% SnO_2 in each segment for both targets was employed, respectively. The exact target geometries can be found in References[24,25,45]. The presence of tin is necessary to facilitate the growth of the Ga_2O_3 based layers in the metastable orthorhombic modification for the PLD deposition method[18–20,23]. However, no significant amount of tin is incorporated during growth, such that this species only serves as surfactant or catalyst to stabilize the κ-phase and not as a dopant. The target powders (all Alfa Aesar) In_2O_3 (99.994 % purity), Al_2O_3 (99.997 % purity), Ga_2O_3 (99.999 % purity), SnO_2 (99.9 % purity) and MgO (99.998 % purity) were ball-milled, cold pressed and sintered in air at ~1650°C for 6 hours (MgO), 1550°C for 72 hours ($(In,Ga)_2O_3$) or 1350°C for 72 hours ($(Al,Ga)_2O_3$ and Ga_2O_3) in the respective mixture and segmentation. The PLD system employs a KrF excimer laser (Coherent LPX Pro 305 F) operating at 248 nm wavelength and 650 mJ pulse energy. The laser is focused to a size of ~2×6.5 mm^2, resulting in an energy density of ~2.6 J/cm^2 at the target surface. A detailed description of the PLD setup can be found in References[46] and[47]. All samples and layers were deposited on c-sapphire substrates (Crystec) at a laser repetition rate of 10 Hz. The oxygen partial pressure and the growth temperature were set to 0.006 mbar and ~620°C for the samples

containing κ-$(In_xGa_{1-x})_2O_3$ layers and 0.002 mbar and ~620°C for the samples with κ-$(Al_xGa_{1-x})_2O_3$ layers, respectively. The κ-$(In_xGa_{1-x})_2O_3$ alloy layers were grown on a κ-Ga_2O_3 template layer for which 15000 laser pulses were applied on the binary target resulting in a buffer thickness of ~500 nm, while for the κ-$(Al_xGa_{1-x})_2O_3$ samples only 10000 pulses were used for the growth template (thickness ~300 nm). For all subsequent alloy layers, 10000 pulses were applied to the elliptically-segmented targets resulting in alloy layer thicknesses in the range of 150-600 nm depending on the exact composition. A detailed investigation on the growth of the orthorhombic binary as well as alloy thin film layers can be found in References[18,24,25]. The composition of the alloy layers was varied between x_{In}=0-0.27 and x_{Al} = 0-0.55 by the radial position *r* of the PLD laser spot on the target surface. For the MgO dielectric layers on the κ-$(In_xGa_{1-x})_2O_3$ samples, a total of 1500 pulses were applied (layer thickness ~7.5 nm) at an oxygen partial pressure of 0.006 mbar and a temperature of ~620°C. These layers were grown in-situ after the deposition of the alloy layer. The MgO layers on the κ-$(Al_xGa_{1-x})_2O_3$ samples were deposited with a total of 1000 pulses (layer thickness ~5 nm) at an oxygen partial pressure of 3×10^{-4} mbar and a temperature of ~400°C. For these, all κ-$(Al_xGa_{1-x})_2O_3$ samples were deposited with vacuum break in the PLD chamber in a different growth process. The growth of the alloy layers purely in the orthorhombic modification was confirmed by X-ray diffraction (XRD) 2θ-ω scans, where a PANalytical X'pert PRO MRD diffractometer with Cu K_α radiation, using a parabolic mirror and PIXcel^{3D} detector, was employed. Typical XRD scans can be found in Supplementary Figure S1.

Photoelectron Spectroscopy

X-ray photoelectron spectroscopy measurements were performed at Humboldt-Universität zu Berlin, using a JEOL JPS-9030 setup with a base pressure of 3×10^{-9} mbar, employing the K_α radiation of a non-monochromated Al X-ray source (hv=1486.6 eV) for excitation and a hemispherical analyzer to detect the kinetic energy of the emitted electrons. The samples were measured without further surface treatment. The C 1s core level was set to 248.8 eV binding energy for reference.

Results

Elemental composition

While the sampling depth of techniques like energy dispersive X-ray spectroscopy (EDX) or Rutherford backscattering (RBS) is too large to reliably analyze the elemental composition of κ-$(Al,In)_xGa_{2-x}O_3$ thin films epitaxially grown on κ-Ga_2O_3 templates, X-ray photoelectron spectroscopy (XPS) is perfectly suited for that purpose[48]. The sampling depth of this technique is only a couple of nanometers, allowing for a reliable determination of the film composition on substrates containing the same elements. Representative survey spectra of $Al_xGa_{2-x}O_3$ and $In_xGa_{2-x}O_3$ are shown in Supplementary Figure S2. Besides gallium, oxygen, aluminum, indium and adventitious carbon, also a small tin signal could be observed, stemming from the Sn surfactant layer needed to trigger the growth in the κ-phase[18]. A determination of the Al content was done by analyzing the area of the Ga $2p_{3/2}$ and the area of the Al 2p core levels after Shirley background

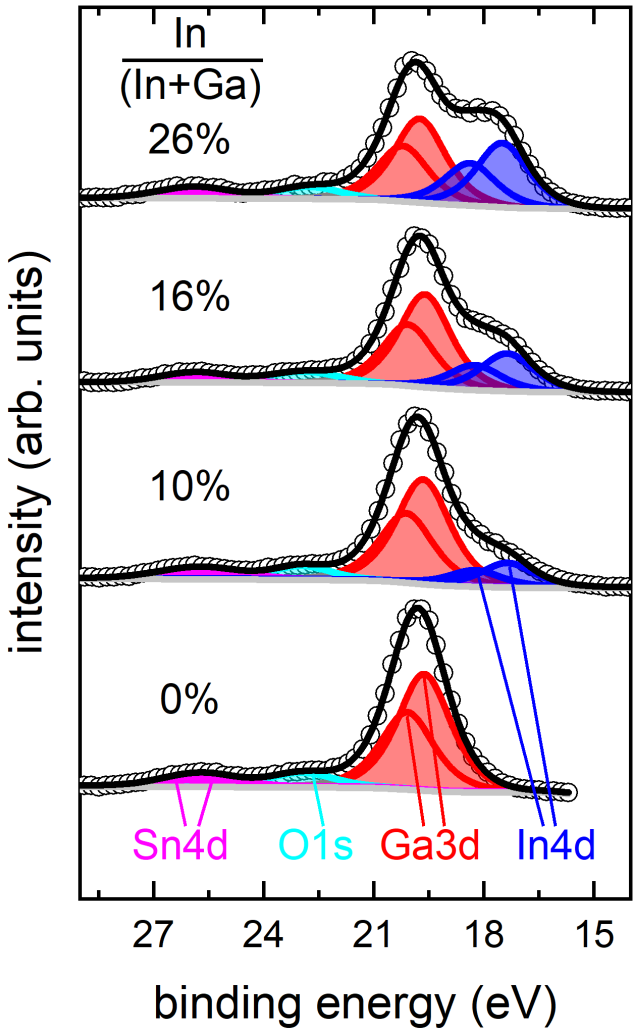

Figure 1: Fits of the Ga 3d and In 4d core level region for different In contents. The In content is determined by comparing the area of the In 4d and the Ga 3d peaks. A small Sn 4d signal is present due to the tin surfactant layer.

subtraction, using sensitivity factors of $S_{Ga\ 2p_{3/2}} = 71.2$ and $S_{Al\ 2p} = 2.3$. Corresponding spectra are shown in Supplementary Figure S3. The In content was more directly determined by fitting the Ga 3d and the In 4d core level spectra as shown in Figure 1. Since the kinetic energies of these core levels are very similar, uncertainties due to different electron mean-free paths are eliminated. For the determination of the In content, sensitivity factors of $S_{Ga\ 3d} = 4.7$ and $S_{In\ 4d} = 9.8$ were employed. Doublet splittings of 0.46 eV and 0.88 eV were used for the Ga 3d and In 4d doublets, respectively. Here again a small contribution from the Sn surfactant layer can be seen as the Sn 4d core level. All In and Al contents are summarized in Supplementary Table I.

Valence band offset determination

For the determination of valence band offsets by XPS one employs the fact that the energy difference between the valence band maximum and a core level is constant for a given material.

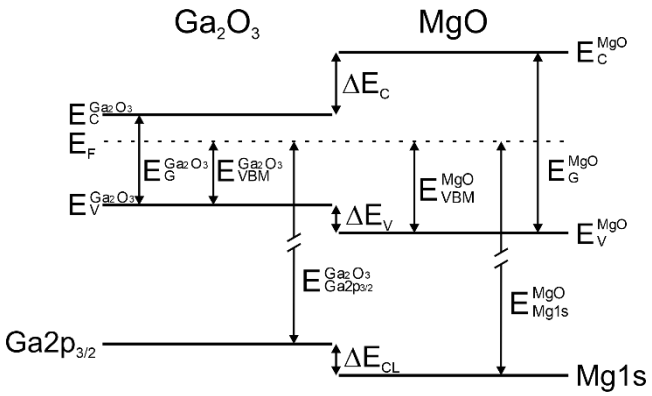

Figure 2: Schematic energy level diagram, demonstrating the energies used to determine the VB offsets ΔE_V.

Therefore, by determining this difference for two pristine materials, one can determine the valence band offset between both materials in a heterostructure by measuring the core level binding energy of both materials. In our case we used the Mg 1s core level of MgO and the Ga $2p_{3/2}$ core level of $([Al,In]_xGa_{1-x})_2O_3$. The employed energy levels are schematically shown for the Ga_2O_3/MgO interface in Figure 2. From these one can determine the VB offset ΔE_V of the materials as follows:[49]

$$\Delta E_V = \Delta E_{CL} - \left(E_{Ga\ 2p_{3/2}}^{([Al,In]_xGa_{1-x})_2O_3} - E_{VBM}^{([Al,In]_xGa_{1-x})_2O_3}\right) + \left(E_{Mg\ 1s}^{MgO} - E_{VBM}^{MgO}\right)$$

Here ΔE_{CL} is the binding energy difference between the Ga $2p_{3/2}$ and the Mg 1s core levels measured at the heterostructure and the energies in brackets are the respective binding energies of the pristine materials. The corresponding core level as well as the valence band spectra are shown for MgO and exemplarily for Ga_2O_3 in Figure 3. The core level positions were determined by fitting with a Voigt-peak after Shirley-background subtraction (uncertainty ≈±25 meV) and the VB onsets were determined from linear extrapolation of the leading edge to the background (uncertainty ≈±75 meV), as indicated by the two red lines in Figure 3 b) and d). The binding energy of all spectra was referenced to the C 1s signal of adventitious carbon, set to 248.8 eV. However, it should be noted that only the energy difference plays a role for the VB offset determination, not the absolute energy position. The measured core level binding energies, valence band onsets and the thereby calculated valence band offsets are summarized in Table I in the SI for all In and Al contents.

Band gap determination from XPS

It has been demonstrated that the band gap of wide band gap materials can be obtained from XPS measurements, by analyzing the onset of the inelastic background at the high binding energy side

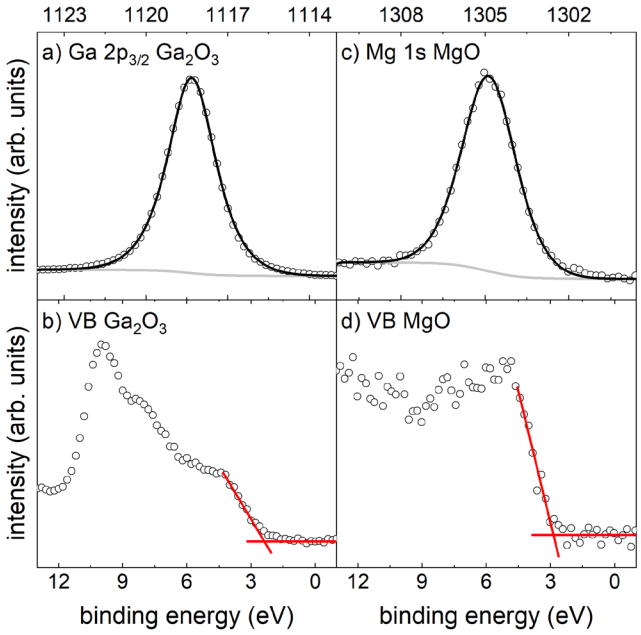

Figure 3: Exemplary core level and valence band spectra of Ga_2O_3 [a) and b)] and MgO [c) and d)]. The core level position is determined after Shirley-background correction and fitting with a Voigt-peak. The valence band onset is determined from a linear extrapolation of the leading edge to the background, as indicated by the two red lines. The two peaks in the Ga_2O_3 VB spectrum at 8 and 10 eV binding energy are satellites from the Ga 3d core level, due to the non-monochromated X-ray excitation.

of a strong core level peak[50–52]. This is because the energetically lowest inelastic scattering that a photoelectron can experience on its way to the surface is the excitation of an electron from the valence band to the conduction band. However, the probability for this scattering event is low and therefore as well the intensity of the inelastic background, which makes prolonged acquisition time necessary for an adequate signal-to-noise ratio. For the band gap determination in this study, we used the O 1s core level, as exemplarily shown in Figure 4 a) for $Al_{0.72}Ga_{1.28}O_3$. However, it should be noted that in principle every core level could be used for this purpose. Figure 4 b) shows a zoom into the background region of the O 1s core level, as indicated by the black box in Figure 4 a). The x-axis here is relative binding energy with respect to the O 1s peak position. A linear extrapolation of the onset of the inelastic background to the constant background gives a band gap of 5.7 eV in the case of $Al_{0.72}Ga_{1.28}O_3$. The determined band gap values for all In and Al compositions are summarized in Supplementary Figure S4 and are in agreement with recently determined values from transmission spectroscopy[24,25]. It should be mentioned that for higher In contents the band gap determined by this method might be overestimated, as the onset of the inelastic background and the core level peak start to partially overlap, making a determination of the constant background difficult. For MgO the band gap determination was a bit more involved, as the O 1s peak consisted of two components [see Supplementary Figure S5 a)]. One at 532.28 eV, which can

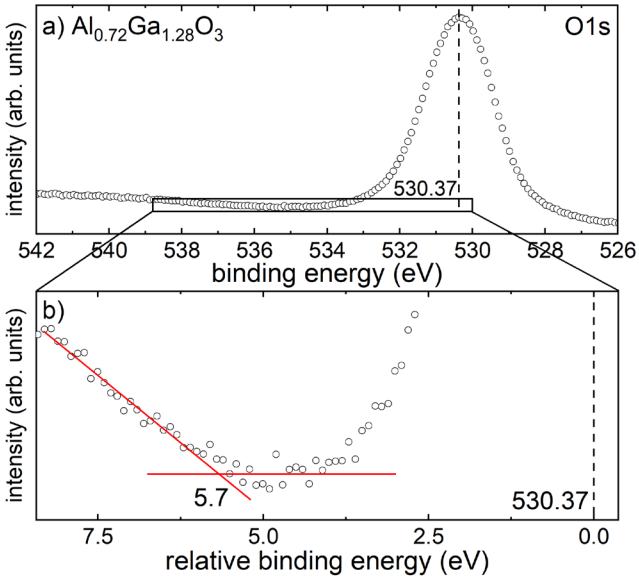

Figure 4: a) O1s core level spectrum of $Al_{0.72}Ga_{1.28}O_3$. The O1s peak position is at 530.37 eV binding energy. b) Zoom into the inelastic background region marked in a). The distance of the onset of the inelastic background, as determined from linear extrapolation as marked in red, to the O1s core level position corresponds to the band gap of the material, which is 5.7 eV in this case.

be attributed to Mg bound to –OH groups at the surface [53–56]. Referencing the inelastic background onset to this peak would lead to a severe underestimation of the band gap. A second peak at 530.42 eV can be attributed to Mg bound to bulk oxygen. Referenced to this peak, the inelastic background onset yields a band gap of 7.7 eV, in good agreement with literature[57,58].

Discussion

The measured band positions of κ-$([Al,In]_xGa_{1-x})_2O_3$ with respect to the MgO bands are summarized for all measured In and Al contents in Figure 5. The CB values as calculated from band gaps determined by transmission experiments[23,24] are shown for comparison as well and are in good agreement. We find that both κ-$(Al_xGa_{1-x})_2O_3$ and κ-$(In_xGa_{1-x})_2O_3$ form a type I heterostructure with MgO. Conduction band offsets of at least 1.4 eV for all compositions provide excellent carrier confinement for electrons exceeding the required 1 eV recommended in literature for MOS transistors[59]. The magnitude of these offsets is similar to those of established dielectrics such as SiO_2, Al_2O_3, HfO_2 or $HfSiO_4$ to various other polymorphs of the $(Al_xGa_{1-x})_2O_3/(In_xGa_{1-x})_2O_3$ alloy systems[60–62]. Therefore, this material might be a promising alternative to these established gate dielectrics in HEMT or other field-effect transistor applications based on Ga_2O_3, as also recently suggested for the monoclinic modification[63]. The valence band offsets are comparably small and no correlation could be found between the offset magnitude and the Al or In content. A much weaker change in the valence band offset compared to the evolution of the

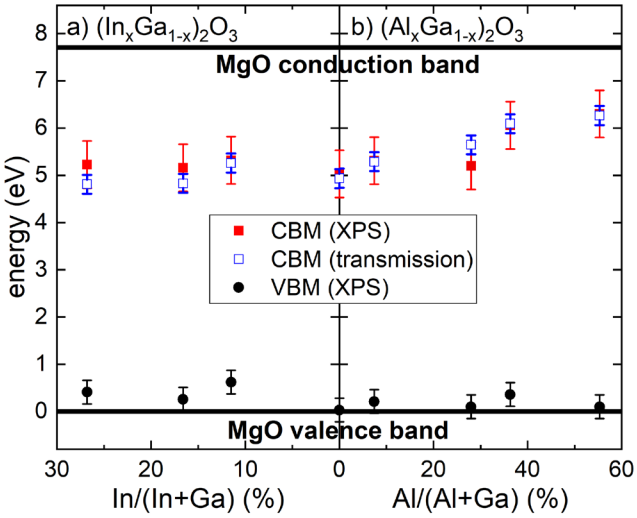

Figure 5: Summary of the energy levels at the a) $(In_xGa_{1-x})_2O_3$/MgO interface and b) at the $(Al_xGa_{1-x})_2O_3$/MgO interface as determined from XPS (red) and transmission[23,24] (blue) measurements. The measured energy levels render the $(Al_xGa_{1-x})_2O_3$/$(In_xGa_{1-x})_2O_3$/$(Al_xGa_{1-x})_2O_3$ a promising heterostructure for quantum wells.

conduction band has been found also for mist-CVD grown κ-$(Al_xGa_{1-x})_2O_3$ films. Notably, a similar trend in the valence band offsets has also already been observed for other polymorphs of the alloy systems, such as the monoclinic β- as well as cubic γ-$(Al_xGa_{1-x})_2O_3$ alloy[60] and the $(In_xGa_{1-x})_2O_3$ alloy in monoclinic or X-ray amorphous modification[64]. DFT calculations further predicted the same flat evolution of the valence band maximum, both for the monoclinic β- as well as the rhombohedral α-phase of the $(Al_xGa_{1-x})_2O_3$ alloy in the complete composition range between Ga_2O_3 and Al_2O_3 in the respective modification[65]. This behavior therefore might not be an exclusive property of the orthorhombic modification, but seems to be the case for all known modifications of the alloy phases of Ga_2O_3. However, there are also reports on band offsets of SiO_2 or HfO_2 to β-$(Al_xGa_{1-x})_2O_3$ thin films, where the valence band offsets are changing much more drastically over a similar composition range of up to 53 at. % aluminum[59,62]. One might therefore be cautious when comparing band offsets in literature even for identical dielectric/semiconductor combinations. Looking at the energy position, one can assume that $(Al_xGa_{1-x})_2O_3$/$(In_xGa_{1-x})_2O_3$/$(Al_xGa_{1-x})_2O_3$ in the orthorhombic modification could render a promising heterostructure for quantum wells with applications as QWIPs or even in HEMT structures. Subniveau transition energies in the conduction band of QWs can therefore be tuned up to a value of 1.1 eV such that detectable wavelengths from the far IR up to the visible might be covered by QWIPs in the investigated composition range.

Conclusion

In summary, by XPS measurements we determined band offsets as well as band gaps of the $([Al,In]_xGa_{1-x})_2O_3$ alloy system in the metastable orthorhombic modification over a broad composition range of up to $x_{In} \leq 0.26$ and $x_{Al} \leq 0.55$. The corresponding thin films were grown by pulsed laser deposition. The employed reference dielectric MgO forms a type I heterostructure to the alloy thin films for all investigated compositions and provides excellent electron confinement with conduction band offsets of at least 1.4 eV. However, valence band offsets of only up to 0.3 eV were determined, such that hole confinement might be an issue. This report is to date the most conclusive investigation on band offsets of the alloy systems in the widest range of compositions for the metastable orthorhombic modification of Ga_2O_3. Our results render this material a promising alternative as gate dielectric for $([Al,In]_xGa_{1-x})_2O_3$ MOS structures, where typically electrons are the majority charge carriers since p-type doping seems not to be feasible in Ga_2O_3. We further found a negligible change in the energy position of the valence band maximum of the alloy layers with increasing aluminum or indium content, such that the conduction band offsets are mainly determined by the evolution of the band gap. A maximum value of this offset of 1.1 eV in combination with the expected polarization jumps at heterointerfaces and the possibility of polarization doping renders the alloy systems in the orthorhombic modification a promising alternative for applications as heterostructures in QWIPs or HEMTs. Especially in QWIPs, this would allow for tunable transition energies from the IR to the visible spectral range.

Acknowledgements

We thank Gabriele Ramm and Monika Hahn for PLD target fabrication as well as Jörg Lenzner for EDX measurements. We are also indebted to Holger Hochmuth for the implementation of VCCS PLD in the growth setup in Leipzig. The work in Berlin was funded by the Deutsche Forschungsgemeinschaft (DFG) - Projektnummer 182087777 - SFB 951. The work in Leipzig was supported by the European Social Fund within the Young Investigator Group ”Oxide Heterostructures” (SAB 100310460). M.K. further acknowledges the Leipzig School for Natural Sciences BuildMoNa.

Associated Content

Supporting Information

Table with all band offsets, XRD 2Θ–ω scans for $([Al,In]_xGa_{1-x})_2O_3$, XPS survey spectra, Ga2p3/2 and Al2p core levels, summary of determined band gaps, O1s loss spectroscopy of MgO

References

(1) Higashiwaki, M.; Sasaki, K.; Murakami, H.; Kumagai, Y.; Koukitu, A.; Kuramata, A.; Masui, T.; Yamakoshi, S. Recent Progress in Ga_2O_3 Power Devices. *Semicond. Sci. Technol.* **2016**, *31* (3), 034001.

(2) Pearton, S. J.; Yang, J.; Cary, P. H.; Ren, F.; Kim, J.; Tadjer, M. J.; Mastro,

M. A. A Review of Ga_2O_3 Materials, Processing, and Devices. *Appl. Phys. Rev.* **2018**, *5* (1), 011301.

(3) von Wenckstern, H. Group-III Sesquioxides: Growth, Physical Properties and Devices. *Adv. Electron. Mater.* **2017**, *3* (9), 1600350.

(4) Sepanov, S. I.; Nikolaev, V. I.; Bougrov, V. E.; Romanov, A. E. Gallium Oxide: Properties and Applications - a Review. *Rev. Adv. Mater. Sci.* **2016**, *44*, 63–86.

(5) Kim, J.; Tahara, D.; Miura, Y.; Kim, B. G. First-Principle Calculations of Electronic Structures and Polar Properties of (κ,ε)-Ga_2O_3. *Appl. Phys. Express* **2018**, *11* (6), 061101.

(6) Shimada, K. First-Principles Study of Crystal Structure, Elastic Stiffness Constants, Piezoelectric Constants, and Spontaneous Polarization of Orthorhombic $Pna2_1$-M_2O_3 (M = Al, Ga, In, Sc, Y). *Mater. Res. Express* **2018**, *5* (3), 036502.

(7) Maccioni, M. B.; Fiorentini, V. Phase Diagram and Polarization of Stable Phases of $(Ga_{1-x}In_x)_2O_3$. *Appl. Phys. Express* **2016**, *9* (4), 041102.

(8) Lähnemann, J.; Brandt, O.; Jahn, U.; Pfüller, C.; Roder, C.; Dogan, P.; Grosse, F.; Belabbes, A.; Bechstedt, F.; Trampert, A.; Geelhaar, L. Direct Experimental Determination of the Spontaneous Polarization of GaN. *Phys. Rev. B* **2012**, *86* (8), 081302.

(9) Kuzuhara, M.; Asubar, J. T.; Tokuda, H. AlGaN/GaN High-Electron-Mobility Transistor Technology for High-Voltage and Low-on-Resistance Operation. *Jpn. J. Appl. Phys.* **2016**, *55* (7), 070101.

(10) Pengelly, R. S.; Wood, S. M.; Milligan, J. W.; Sheppard, S. T.; Pribble, W. L. A Review of GaN on SiC High Electron-Mobility Power Transistors and MMICs. *IEEE Trans. Microw. Theory Tech.* **2012**, *60* (6), 1764–1783.

(11) Beeler, M.; Trichas, E.; Monroy, E. III-Nitride Semiconductors for Intersubband Optoelectronics: A Review. *Semicond. Sci. Technol.* **2013**, *28* (7), 074022.

(12) Zhang, Y.; Xia, Z.; McGlone, J.; Sun, W.; Joishi, C.; Arehart, A. R.; Ringel, S. A.; Rajan, S. Evaluation of Low-Temperature Saturation Velocity in β-$(Al_xGa_{1-x})_2O_3$/Ga_2O_3 Modulation-Doped Field-Effect Transistors. *IEEE Trans. Electron Devices* **2019**, *66* (3), 1574–1578.

(13) Zhang, Y.; Neal, A.; Xia, Z.; Joishi, C.; Johnson, J. M.; Zheng, Y.; Bajaj, S.; Brenner, M.; Dorsey, D.; Chabak, K.; Jessen, G.; Hwang, J.; Mou, S.;

Heremans, J. P.; Rajan, S. Demonstration of High Mobility and Quantum Transport in Modulation-Doped β-$(Al_xGa_{1-x})_2O_3/Ga_2O_3$ Heterostructures. *Appl. Phys. Lett.* **2018**, *112* (17), 173502.

(14) Zhang, Y.; Joishi, C.; Xia, Z.; Brenner, M.; Lodha, S.; Rajan, S. Demonstration of β-$(Al_xGa_{1-x})_2O_3$ Double Heterostructure Field Effect Transistors. *Appl. Phys. Lett.* **2018**, *112* (23), 233503.

(15) Oshima, T.; Kato, Y.; Kawano, N.; Kuramata, A.; Yamakoshi, S.; Fujita, S.; Oishi, T.; Kasu, M. Carrier Confinement Observed at Modulation-Doped β-$(Al_xGa_{1-x})_2O_3/Ga_2O_3$ Heterojunction Interface. *Appl. Phys. Express* **2017**, *10* (3), 035701.

(16) Krishnamoorthy, S.; Xia, Z.; Joishi, C.; Zhang, Y.; McGlone, J.; Johnson, J.; Brenner, M.; Arehart, A. R.; Hwang, J.; Lodha, S.; Rajan, S. Modulation-Doped β-$(Al_{0.2}Ga_{0.8})_2O_3/Ga_2O_3$ Field-Effect Transistor. *Appl. Phys. Lett.* **2017**, *111* (2), 023502.

(17) Kaun, S. W.; Wu, F.; Speck, J. S. β -$(Al_xGa_{1-x})_2O_3/Ga_2O_3$ (010) Heterostructures Grown on β-Ga_2O_3 (010) Substrates by Plasma-Assisted Molecular Beam Epitaxy. *J. Vac. Sci. Technol. A Vacuum, Surfaces, Film.* **2015**, *33* (4), 041508.

(18) Kneiß, M.; Hassa, A.; Splith, D.; Sturm, C.; Von Wenckstern, H.; Schultz, T.; Koch, N.; Lorenz, M.; Grundmann, M. Tin-Assisted Heteroepitaxial PLD-Growth of κ-Ga_2O_3 Thin Films with High Crystalline Quality. *APL Mater.* **2019**, *7* (2), 022516.

(19) Orita, M.; Hiramatsu, H.; Ohta, H.; Hirano, M.; Hosono, H. Preparation of Highly Conductive, Deep Ultraviolet Transparent β-Ga_2O_3 Thin Film at Low Deposition Temperatures. *Thin Solid Films* **2002**, *411* (1), 134–139.

(20) Matsuzaki, K.; Hiramatsu, H.; Nomura, K.; Yanagi, H.; Kamiya, T.; Hirano, M.; Hosono, H. Growth, Structure and Carrier Transport Properties of Ga_2O_3 Epitaxial Film Examined for Transparent Field-Effect Transistor. *Thin Solid Films* **2006**, *496* (1), 37–41.

(21) Matsuzaki, K.; Yanagi, H.; Kamiya, T.; Hiramatsu, H.; Nomura, K.; Hirano, M.; Hosono, H. Field-Induced Current Modulation in Epitaxial Film of Deep-Ultraviolet Transparent Oxide Semiconductor Ga_2O_3. *Appl. Phys. Lett.* **2006**, *88* (9), 092106.

(22) Zhao, X.; Zhi, Y.; Cui, W.; Guo, D.; Wu, Z.; Li, P.; Li, L.; Tang, W. Characterization of Hexagonal ε-$Ga_{1.8}Sn_{0.2}O_3$ Thin Films for Solar-Blind Ultraviolet Applications. *Opt. Mater. (Amst).* **2016**, *62*, 651–654.

(23) Hassa, A.; von Wenckstern, H.; Splith, D.; Sturm, C.; Kneiß, M.; Prozheeva, V.; Grundmann, M. Structural, Optical, and Electrical Properties of Orthorhombic κ-$(In_xGa_{1-x})_2O_3$ Thin Films. *APL Mater.* **2019**, *7* (2), 022525.

(24) Storm, P.; Kneiß, M.; Hassa, A.; Schultz, T.; Splith, D.; Koch, N.; Lorenz, M.; Grundmann, M. Epitaxial κ-$(Al_xGa_{1-x})_2O_3$ Thin Films and Heterostructures Grown by Tin-Assisted VCCS-PLD. *APL Mater.* **2019**, *7* (11), 1–12.

(25) Kneiß, M.; Hassa, A.; Splith, D.; Sturm, C.; von Wenckstern, H.; Lorenz, M.; Grundmann, M. Epitaxial Stabilization of Single Phase κ -$(In_xGa_{1-x})_2O_3$ Thin Films up to x = 0.28 on c-Sapphire and κ -Ga_2O_3 (001) Templates by Tin-Assisted VCCS-PLD. *APL Mater.* **2019**, *7* (10), 101102.

(26) Yao, Y.; Okur, S.; Lyle, L. A. M.; Tompa, G. S.; Salagaj, T.; Sbrockey, N.; Davis, R. F.; Porter, L. M. Growth and Characterization of α-, β-, and ϵ-Phases of Ga_2O_3 Using MOCVD and HVPE Techniques. *Mater. Res. Lett.* **2018**, *6* (5), 268–275.

(27) Oshima, Y.; Víllora, E. G.; Matsushita, Y.; Yamamoto, S.; Shimamura, K. Epitaxial Growth of Phase-Pure ε-Ga_2O_3 by Halide Vapor Phase Epitaxy. *J. Appl. Phys.* **2015**, *118* (8), 085301.

(28) Sun, H.; Li, K.-H.; Castanedo, C. G. T.; Okur, S.; Tompa, G. S.; Salagaj, T.; Lopatin, S.; Genovese, A.; Li, X. HCl Flow-Induced Phase Change of α-, β-, and ε-Ga_2O_3 Films Grown by MOCVD. *Cryst. Growth Des.* **2018**, *18* (4), 2370–2376.

(29) Zhuo, Y.; Chen, Z.; Tu, W.; Ma, X.; Pei, Y.; Wang, G. β-Ga_2O_3 versus ε-Ga_2O_3 : Control of the Crystal Phase Composition of Gallium Oxide Thin Film Prepared by Metal-Organic Chemical Vapor Deposition. *Appl. Surf. Sci.* **2017**, *420*, 802–807.

(30) Fornari, R.; Pavesi, M.; Montedoro, V.; Klimm, D.; Mezzadri, F.; Cora, I.; Pécz, B.; Boschi, F.; Parisini, A.; Baraldi, A.; Ferrari, C.; Gombia, E.; Bosi, M. Thermal Stability of ε-Ga_2O_3 Polymorph. *Acta Mater.* **2017**, *140*, 411–416.

(31) Mezzadri, F.; Calestani, G.; Boschi, F.; Delmonte, D.; Bosi, M.; Fornari, R. Crystal Structure and Ferroelectric Properties of ε-Ga_2O_3 Films Grown on (0001)-Sapphire. *Inorg. Chem.* **2016**, *55* (22), 12079–12084.

(32) Boschi, F.; Bosi, M.; Berzina, T.; Buffagni, E.; Ferrari, C.; Fornari, R. Hetero-Epitaxy of ε-Ga_2O_3 Layers by MOCVD and ALD. *J. Cryst. Growth* **2016**, *443*, 25–30.

(33) Xia, X.; Chen, Y.; Feng, Q.; Liang, H.; Tao, P.; Xu, M.; Du, G. Hexagonal Phase-Pure Wide Band Gap ε-Ga_2O_3 Films Grown on 6H-SiC Substrates by Metal Organic Chemical Vapor Deposition. *Appl. Phys. Lett.* **2016**, *108* (20), 202103.

(34) Gottschalch, V.; Merker, S.; Blaurock, S.; Kneiß, M.; Teschner, U.; Grundmann, M.; Krautscheid, H. Heteroepitaxial Growth of α-, β-, γ- and κ-Ga_2O_3 Phases by Metalorganic Vapor Phase Epitaxy. *J. Cryst. Growth* **2019**, *510*, 76–84.

(35) Mulazzi, M.; Reichmann, F.; Becker, A.; Klesse, W. M.; Alippi, P.; Fiorentini, V.; Parisini, A.; Bosi, M.; Fornari, R. The Electronic Structure of ε-Ga_2O_3. *APL Mater.* **2019**, *7* (2), 022522.

(36) Parisini, A.; Bosio, A.; Montedoro, V.; Gorreri, A.; Lamperti, A.; Bosi, M.; Garulli, G.; Vantaggio, S.; Fornari, R. Si and Sn Doping of ε-Ga_2O_3 Layers. *APL Mater.* **2019**, *7* (3), 031114.

(37) Cora, I.; Mezzadri, F.; Boschi, F.; Bosi, M.; Čaplovičová, M.; Calestani, G.; Dódony, I.; Pécz, B.; Fornari, R. The Real Structure of ε-Ga_2O_3 and Its Relation to κ-Phase. *CrystEngComm* **2017**, *19* (11), 1509–1516.

(38) Nishinaka, H.; Miyauchi, N.; Tahara, D.; Morimoto, S.; Yoshimoto, M. Incorporation of Indium into ε-Gallium Oxide Epitaxial Thin Films Grown via Mist Chemical Vapour Deposition for Bandgap Engineering. *CrystEngComm* **2018**, *20* (13), 1882–1888.

(39) Nishinaka, H.; Tahara, D.; Yoshimoto, M. Heteroepitaxial Growth of ε-Ga_2O_3 Thin Films on Cubic (111) MgO and (111) Yttria-Stablized Zirconia Substrates by Mist Chemical Vapor Deposition. *Jpn. J. Appl. Phys.* **2016**, *55* (12), 1202BC.

(40) Tahara, D.; Nishinaka, H.; Morimoto, S.; Yoshimoto, M. Heteroepitaxial Growth of ϵ-$(Al_xGa_{1-x})_2O_3$ Alloy Films on c -Plane AlN Templates by Mist Chemical Vapor Deposition. *Appl. Phys. Lett.* **2018**, *112* (15), 152102.

(41) Tahara, D.; Nishinaka, H.; Morimoto, S.; Yoshimoto, M. Heteroepitaxial Growth of ϵ-Ga_2O_3 Thin Films on Cubic (111) GGG Substrates by Mist Chemical Vapor Deposition. In *IMFEDK 2017 - 2017 International Meeting for Future of Electron Devices, Kansai*; IEEE, 2017; pp 48–49.

(42) Tahara, D.; Nishinaka, H.; Morimoto, S.; Yoshimoto, M. Stoichiometric Control for Heteroepitaxial Growth of Smooth ϵ-Ga_2O_3 Thin Films on c-Plane AlN Templates by Mist Chemical Vapor Deposition. *Jpn. J. Appl. Phys.* **2017**, *56* (7), 078004.

(43) Vogt, P.; Brandt, O.; Riechert, H.; Lähnemann, J.; Bierwagen, O. Metal-Exchange Catalysis in the Growth of Sesquioxides: Towards Heterostructures of Transparent Oxide Semiconductors. *Phys. Rev. Lett.* **2017**, *119* (19), 196001.

(44) Kracht, M.; Karg, A.; Schörmann, J.; Weinhold, M.; Zink, D.; Michel, F.; Rohnke, M.; Schowalter, M.; Gerken, B.; Rosenauer, A.; Klar, P. J.; Janek, J.; Eickhoff, M. Tin-Assisted Synthesis of ε-Ga_2O_3 by Molecular Beam Epitaxy. *Phys. Rev. Appl.* **2017**, *8* (5), 054002.

(45) Kneiß, M.; Storm, P.; Benndorf, G.; Grundmann, M.; von Wenckstern, H. Combinatorial Material Science and Strain Engineering Enabled by Pulsed Laser Deposition Using Radially Segmented Targets. *ACS Comb. Sci.* **2018**, *20* (11), 643–652.

(46) Lorenz, M. Pulsed Laser Deposition of ZnO-Based Thin Films; Springer, Berlin, Heidelberg, 2008; pp 303–357.

(47) Lorenz, M.; Hochmuth, H.; Grüner, C.; Hilmer, H.; Lajn, A.; Spemann, D.; Brandt, M.; Zippel, J.; Schmidt-Grund, R.; Von Wenckstern, H.; Grundmann, M. Oxide Thin Film Heterostructures on Large Area, with Flexible Doping, Low Dislocation Density, and Abrupt Interfaces: Grown by Pulsed Laser Deposition. *Laser Chem.* **2010**, *2010*, 1–27.

(48) Ebnesajjad, S. Surface and Material Characterization Techniques. In *Handbook of Adhesives and Surface Preparation*; William Andrew Publishing, 2011; pp 31–48.

(49) Chen, S.; Pan, X.; Xu, C.; Huang, J.; Ye, Z. X-Ray Photoelectron Spectroscopy Study of Energy-Band Alignments of ZnO on Buffer Layer Lu_2O_3. *Phys. Lett. A* **2016**, *380* (7–8), 970–972.

(50) Miyazaki, S.; Nishimura, H.; Fukuda, M.; Ley, L.; Ristein, J. Structure and Electronic States of Ultrathin SiO_2 Thermally Grown on Si(100) and Si(111) Surfaces. *Appl. Surf. Sci.* **1997**, *113–114*, 585–589.

(51) Miyazaki, S. Characterization of High-k Gate Dielectric/Silicon Interfaces. In *Applied Surface Science*; 2002; Vol. 190, pp 66–74.

(52) Nichols, M. T.; Li, W.; Pei, D.; Antonelli, G. A.; Lin, Q.; Banna, S.; Nishi, Y.; Shohet, J. L. Measurement of Bandgap Energies in Low-k Organosilicates. *J. Appl. Phys.* **2014**, *115* (9), 094105.

(53) Wu, J.; Wang, L.; Wang, J.; Du, Y.; Li, Y. MgO-Based Nanosheets Loaded with $Zn_xMg_{1-x}O$ Nanoparticles with UV Light-Driven Photocatalytic Performance. *Funct. Mater. Lett.* **2017**, *10* (06), 1750072.

(54) Terauchi, M.; Hashimoto, J.; Nishitani, H.; Fukui, Y.; Okafuji, M.; Yamashita, H.; Hayata, H.; Okuma, T.; Yamanishi, H.; Nishitani, M.; Kitagawa, M. High-Performance MgO Thin Films for PDPs with a High-Rate Sputtering-Deposition Process. *J. Soc. Inf. Disp.* **2008**, *16* (12), 1195.

(55) Lee, J. H.; Eun, J. H.; Park, S. Y.; Kim, S. G.; Kim, H. J. Hydration of r.f. Magnetron Sputtered MgO Thin Films for a Protective Layer in AC Plasma Display Panel. *Thin Solid Films* **2003**, *435* (1–2), 95–101.

(56) Newberg, J. T.; Starr, D. E.; Yamamoto, S.; Kaya, S.; Kendelewicz, T.; Mysak, E. R.; Porsgaard, S.; Salmeron, M. B.; Brown, G. E.; Nilsson, A.; Bluhm, H. Formation of Hydroxyl and Water Layers on MgO Films Studied with Ambient Pressure XPS. *Surf. Sci.* **2011**, *605* (1–2), 89–94.

(57) R. C. Whited and W. C. Walker. Exciton Spectra of CaO and MgO. *Phys. Rev. Lett.* **1969**, *22* (26), 1428–1430.

(58) Heo, S.; Cho, E.; Lee, H.-I.; Park, G. S.; Kang, H. J.; Nagatomi, T.; Choi, P.; Choi, B.-D. Band Gap and Defect States of MgO Thin Films Investigated Using Reflection Electron Energy Loss Spectroscopy. *J. Chem. Phys.* **2015**, *5*, 77167.

(59) Feng, Z.; Feng, Q.; Zhang, J.; Zhang, C.; Zhou, H.; Li, X.; Huang, L.; Xu, L.; Hu, Y.; Zhao, S.; Hao, Y. Band Alignments of SiO_2 and HfO_2 Dielectrics with $(Al_xGa_{1-x})_2O_3$ Film ($0 \leq x \leq 0.53$) Grown on Ga_2O_3 Buffer Layer on Sapphire. *J. Alloys Compd.* **2018**, *745*, 292–298.

(60) Fares, C.; Kneiß, M.; von Wenckstern, H.; Tadjer, M.; Ren, F.; Lambers, E.; Grundmann, M.; Pearton, S. J. Band Alignment of Atomic Layer Deposited SiO_2 and Al_2O_3 on $(Al_xGa_{1-x})_2O_3$ for x = 0.2-0.65. *ECS J. Solid State Sci. Technol.* **2019**, *8* (6), 351–356.

(61) Fares, C.; Ren, F.; Lambers, E.; Hays, D. C.; Gila, B. P.; Pearton, S. J. Valence- and Conduction-Band Offsets for Atomic-Layer-Deposited Al_2O_3 on (010) $(Al_{0.14}Ga_{0.86})_2O_3$. *J. Electron. Mater.* **2019**, *48* (3), 1568–1573.

(62) Feng, Z.; Feng, Q.; Zhang, J.; Li, X.; Li, F.; Huang, L.; Chen, H.-Y.; Lu, H.-L.; Hao, Y. Band Alignment of $SiO_2/(Al_x\ Ga_{1-x})_2O_3$ ($0 \leq x \leq 0.49$) Determined by X-Ray Photoelectron Spectroscopy. *Appl. Surf. Sci.* **2018**, *434*, 440–444.

(63) Liu, Z.; Yu, J.; Li, P.; Wang, X.; Zhi, Y.; Chu, X.; Wang, X.; Li, H.; Wu, Z.; Tang, W. Band Alignments of β-Ga_2O_3 with MgO, Al_2O_3 and $MgAl_2O_4$ Measured by X-Ray Photoelectron Spectroscopy. *J. Phys. D. Appl. Phys.* **2019**, *52* (29), 295104.

(64) Fares, C.; Kneiß, M.; von Wenckstern, H.; Grundmann, M.; Tadjer, M.; Ren,

F.; Lambers, E.; Pearton, S. J. Valence Band Offsets for ALD SiO_2 and Al_2O_3 on $(In_xGa_{1-x})_2O_3$ for x = 0.25–0.74. *APL Mater.* **2019**, *7* (7), 071115.

(65) Wang, T.; Li, W.; Ni, C.; Janotti, A. Band Gap and Band Offset of Ga_2O_3 and $(Al_xGa_{1-x})_2O_3$ Alloys. *Phys. Rev. Appl.* **2018**, *10* (1), 011003.

For Table of Contents Only